

## LHCb/LHCf/TOTEM input for astrophysics

V. ZHUKOV<sup>(1)(2)</sup> on behalf of the LHCb COLLABORATION

<sup>(1)</sup> *RWTHA, Aachen University of Technology - Aachen, Germany*

<sup>(2)</sup> *SINP, Moscow State University - Moscow, Russia*

received 6 September 2018

**Summary.** — The impact of recent LHCb, LHCf, and TOTEM results on the cosmic-rays astrophysics and the indirect dark-matter search is discussed.

### 1. – Introduction

For many Dark-Matter (DM) candidates the antiprotons, positrons,  $\gamma$ -rays and neutrinos after DM annihilation can be observed on top of the galactic cosmic-Ray (CR) fluxes [1]. Nuclear interactions of CR with the interstellar gas or the Earth atmosphere is a major background for this indirect dark-matter search. Recent measurements of the CR positrons and antiprotons by the AMS02 [2, 3], and the diffusive  $\gamma$ -rays by the Fermi-LAT [4] demonstrate some deviations from the predicted spectra, where the degree of deviation depends upon uncertainties in the background calculations. These uncertainties can be roughly split into two parts: the astrophysical and nuclear origins. The astrophysical uncertainties are related to the propagation parameters, spectral shape and composition of primary CR at production, distribution of CR sources, and the Inter-Stellar Gas (ISG) and Radiation Field (ISRF) distributions. For kinetic energies below 10 GeV the solar modulation becomes equally important for measurements of local CR. The galactic models based on the isotropic and uniform diffusion, like the Galprop [5], have only a limited number of propagation parameters that can be extracted from the fit to the CR measurements [6]. The universal spectral shape of primary CR is well supported by the advance in acceleration models [7], while the CR source and the inter-stellar medium (ISG+ISRF) distributions can be constrained from the optical and radio measurements.

The nuclear uncertainties are mostly related to the inelastic cross-sections that can be obtained either using different parameterizations, or from simulation models. The parameterization of existing measurements is limited to the visible phase space and requires several assumptions on scaling for extrapolations. The models offer a better ground for these assumptions, but may fail to reproduce details. The models are largely based on the

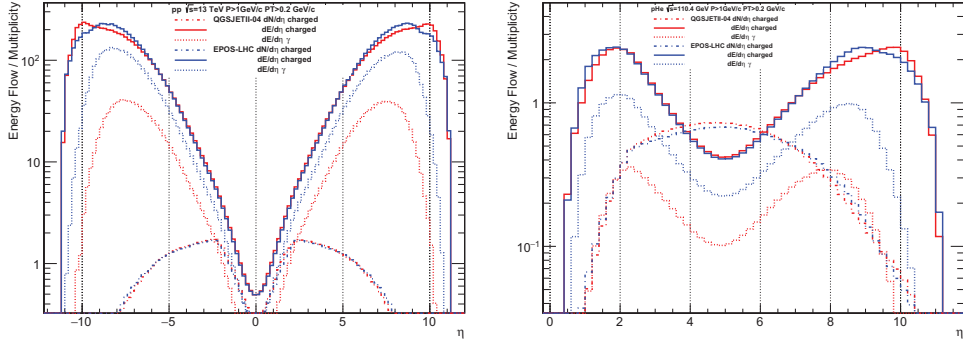


Fig. 1. – Energy flow  $dE/d\eta$  for charged particles and  $\gamma$ , and multiplicity  $dN/d\eta$  of charged particles in  $pp$  collisions at  $\sqrt{s} = 13$  TeV (left) and in the fixed target  $pHe$  interactions at  $\sqrt{s_{NN}} = 110.4$  GeV (right) for two different models: EPOS-LHC [9] and QGSJETII-04 [10]. The particles are selected with  $P > 1$  GeV/ $c$  and  $P_T > 0.2$  GeV/ $c$ .

Reggeon Field Theory (RFT) formalism implemented in various packages [8]. Among them are the EPOS [9] and QGSJET [10] MC simulations, which use a consistent treatment of hard- and soft-pomeron exchanges allowing to predict inelastic cross-sections including soft contributions. Most of CR interactions in space correspond to the large impact parameter collisions with low  $Q^2$ , typical for forward and fixed target measurements, rather than hard central collisions studied in the ATLAS or CMS experiments, which are therefore complemented with forward detectors. The TOTEM tracking stations with  $|\eta| > 3.5$  coverage add up to the CMS tracking coverage of  $|\eta| < 2.4$  [11]. The LHCf neutral particles calorimeters with  $|\eta| > 8.1$  extend the ATLAS calorimeter coverage of  $|\eta| < 4.9$  [12]. The LHCb detector has its own range  $2 < \eta < 5$ , but can also operate in the fixed-target mode increasing the kinematic reach [13]. Figure 1 shows the charged particle multiplicity and energy flows in the  $pp$  collisions at  $\sqrt{s} = 13$  TeV and fixed target  $pHe$  interactions at  $\sqrt{s} = 110.4$  GeV ( $E_{beam} = 6.5$  TeV) *vs.* pseudorapidity, which are calculated with the new versions of EPOS-LHC and QGSJETII-04 models that are tuned to reproduce the LHC run1 and recent Extensive Air Shower (EAS) measurements [14]. The spread in predictions can be interpreted as uncertainties, which can be reduced with new measurements.

In this contribution we review selected results from the LHCb, LHCf and TOTEM experiments, which are important for the validation of CR simulation models and parameterizations. We discuss the implications of these measurements on the antiprotons, diffusive  $\gamma$ -rays and neutrinos production in CR interactions, where the nuclear uncertainties can be important. The production of CR positrons is rather similar, but the nuclear uncertainties can be neglected in comparison with the astrophysical ones [1], hence not considered here. We also briefly review the cross-section measurements, including diffraction.

## 2. – Antiprotons

For the DM annihilation into two quark jets the  $\bar{p}$  component has the largest significance in comparison with positrons,  $\gamma$ -rays or neutrinos. The spectrum of such  $\bar{p}$  is rather broad, with a cutoff near the mass of the DM candidate. The background CR  $\bar{p}$ 's are produced in space mostly from interactions of CR protons  $p$  (90%) and He

with the ISG. Assuming isospin symmetry, about half of the  $\bar{p}$ 's is produced directly in  $AA \rightarrow \bar{p}X$  inelastic collisions, and another half via production and decays of antineutrons  $AA \rightarrow \bar{n}X \rightarrow \bar{p}\nu X$ . The direct production includes the prompt component (about 70%) and the displaced one from the decays of antihyperons  $\bar{\Lambda}(\bar{p}\pi)$ ,  $\bar{\Sigma}(\bar{p}\pi^0)$ . The direct prompt  $\bar{p}$  production in the  $pH$  and  $pHe$  interactions contribute about 20% each to the total antiproton flux at 10–500 GeV. The secondary CR  $\bar{p}$  in this energy range are produced by about 0.1–5 TeV projectiles, close to the LHC beam energies  $E_{beam} = 0.9\text{--}6.5$  TeV ( $\sqrt{s_{NN}} \approx 45\text{--}110$  GeV) [15]. Although the protons are dominant in the CR and ISG, the overall contribution from interactions involving He is significant and increases with energy, exceeding 50% above 1 TeV [16].

There are different parameterizations of the  $\bar{p}$  inclusive cross-section. The old Tan and Yan parameterization [17] used in Galprop is based on the  $\sqrt{s} < 60$  GeV measurements and assumes Feynman scaling. It significantly underpredicts the  $\bar{p}$  production at  $\sqrt{s} > 100$  GeV. More recent parameterizations from di Mauro *et al.* [18], and Winkler [19] accept some scaling violations and include in addition the SPS, RHIC, and LHC measurements. However, the experimental data in the important  $\sqrt{s_{NN}} = 50\text{--}200$  GeV range are missing. The uncertainties in parameterizations are about 30% [18] in comparison to the 10% of astrophysical uncertainties related to the spectral shape of primary CR.

The measurement of the differential  $d\sigma(\bar{p}X)/dp_T dp$  cross-section of prompt  $\bar{p}$  production in fixed target  $pHe$  interactions ( $\sqrt{s} = 110.4$  GeV) was performed at the LHCb [20]. In the fixed tagged mode the inert gas (He, Ne, Ar) can be injected directly into the beam pipe near the LHCb vertex detector and pumped out at  $\pm 20$  m distances. Giving the LHCb  $\eta$  acceptance, such measurements correspond to the target fragmentation region with the negative Feynman parameter  $x_F = x_1 - x_2 = p_L/2\sqrt{s}$  down to  $x_F \approx -0.3$ , where the projectile Bjorken  $x_1 \sim 0$  is much smaller than the target  $x_2 \sim 1$ . The analysis is done in the  $p_T$ - $p$  bins, where the ranges  $0.4 < p_T < 4$  GeV/ $c$  and  $12 < p < 120$  GeV/ $c$  are defined by the LHCb acceptance and particle identification. Since the maximum of the  $\bar{p}$  production is in the central region at rapidity  $y_{beam}/2 \approx 4.8$ , only some part of the CR  $pHe$  interactions phase space is covered by the LHCb acceptance, see fig. 1. The total uncertainties are about 10% for most of the bins, increasing to about 25% for the boundaries at low and high momentum. The absolute luminosity is determined from the  $pe^-$  elastic scattering and gives 6% of correlated systematic. The differential cross-section is compared with the EPOS-LHC, QGSJET-II-04m [15] in fig. 2. Good agreement with the QGSJET and the parameterization [19] is observed, while the EPOS-LHC underestimates prompt antiproton production at high  $p_T$  by about 50% [16]. Despite this, the total  $\bar{p}$  yield in the CR predicted by EPOS-LHC is significantly larger than the QGSJET [21]. This is traced to the large isospin symmetry violation  $\bar{n}/\bar{p} \sim 1.5$  assumed in EPOS-LHC, which still has to be confirmed [22].

The LHCb measurements, together with assumptions on the isospin symmetry and hyperon production, almost exclude the possibility for the DM contribution in the observed antiproton flux [16]. The nuclear uncertainties are reduced to  $\sim 10\%$ , and are comparable now with astrophysical uncertainties [23]. The contribution from hyperons is still under study at LHCb, and the isospin asymmetry can be potentially tested with a deuteron target. Since the CR energy spectrum is strongly falling as  $E^{-2.7}$ , the events with low inelasticity contribute the most. Then the lowering of beam energy down to 1 TeV would move the bulk of the  $\bar{p}$  production into the LHCb acceptance and cover a larger phase space relevant for CR observations in the  $E_{\bar{p}} = 10$  GeV–1 TeV energy range. Another important subject is the nuclear modification factors, which can be studied with different gas targets at LHCb.

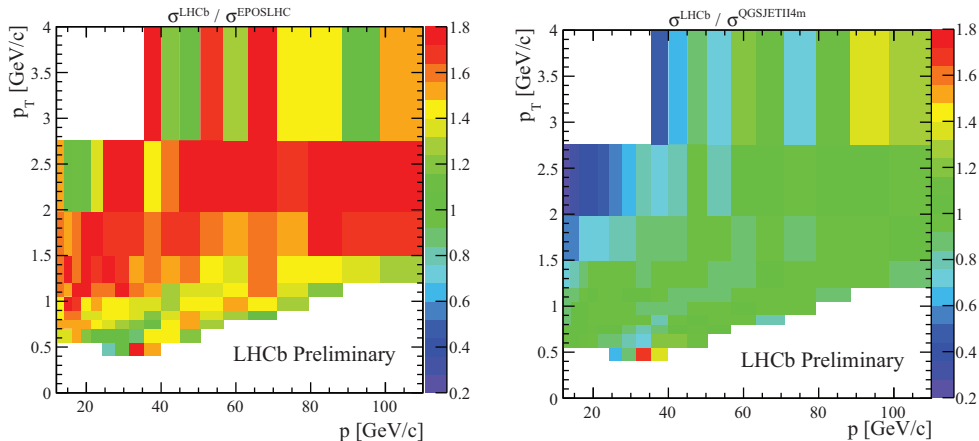


Fig. 2. – LHCb prompt antiproton Data/MC ratios for the EPOS-LHC (left) and QGSJET-II-04 m (right) in the fixed target  $p$ He interactions at  $\sqrt{s} = 110.4$  GeV [20].

### 3. – Diffusive gamma ray

The DM annihilation can result in two distinct signatures in the CR  $\gamma$ -rays spectrum: the continuous contribution similar to  $\bar{p}$  or the peak at the DM mass from the annihilation directly into  $2\gamma(Z/H\gamma)$ . The astrophysical diffusive  $\gamma$ -rays are produced in space via three main channels. The interaction of galactic CR( $p$ , He, . . .)+ISG $\rightarrow\pi^0(\gamma\gamma)$  produces an enhancement in the diffusive  $\gamma$ -rays spectrum peaking at  $E_\gamma \sim 2$  GeV and slowly decreasing at higher energies. Other two production channels are related to the interaction of galactic  $e^\pm$  either with the ISRF via inverse Compton contributing to higher energies, or with the ISG producing  $\gamma$  bremsstrahlung contributing to low energies. The diffusive  $\gamma$ -rays with  $E_\gamma = 1$ –10 GeV are produced by interactions of CR projectiles in the 10–100 GeV energy range, where the local CR spectra are relatively well measured. This makes nuclear uncertainties dominant in this range, while at higher and lower energies most of the diffusive  $\gamma$ -rays are produced from galactic electrons, especially outside the galactic disk. The connection between diffusive  $\gamma$ -rays and galactic CR distribution gives the possibility to validate the galactic propagation model [24]. For this the nuclear uncertainties in the CR+ISG interactions are important at all energies.

The production of  $\gamma$  in  $AA$  collisions is rather different from the centrally produced  $\bar{p}$ , see fig. 1. The  $\gamma$ -rays can be also produced in forward regions, for example from diffractive processes, which complicates the calculations. At  $E_\gamma > 10$  GeV about 20% of the inelastic cross-section is diffraction, while below 10 GeV most of the  $\gamma$ -rays are produced via  $N^*$ ,  $\Delta(1238)$  resonances. The early parameterizations from Stephens and Badhwar [25], Dermer [26], and Kamae *et al.* [27] give about 30% spread in predictions in the 1–100 GeV region [28,29]. The LHC data on the inelastic cross-sections [30] improve parameterization, especially in high-energy region above 100 GeV [31] where scaling is broken, but the validation with direct measurements is needed.

The direct measurements of very forward  $\gamma$  and  $\pi^0$  production in  $pp$  collisions at  $\sqrt{s} = 7$  and 13 TeV were performed at the LHCf for  $E_\gamma > 100$  GeV. The LHCf detector has two calorimeters located at  $\pm 140$  m distances from the ATLAS interaction point after dipole magnets that separate neutral components:  $\gamma$ ,  $\pi^0$  (reconstructed from  $2\gamma$ ),

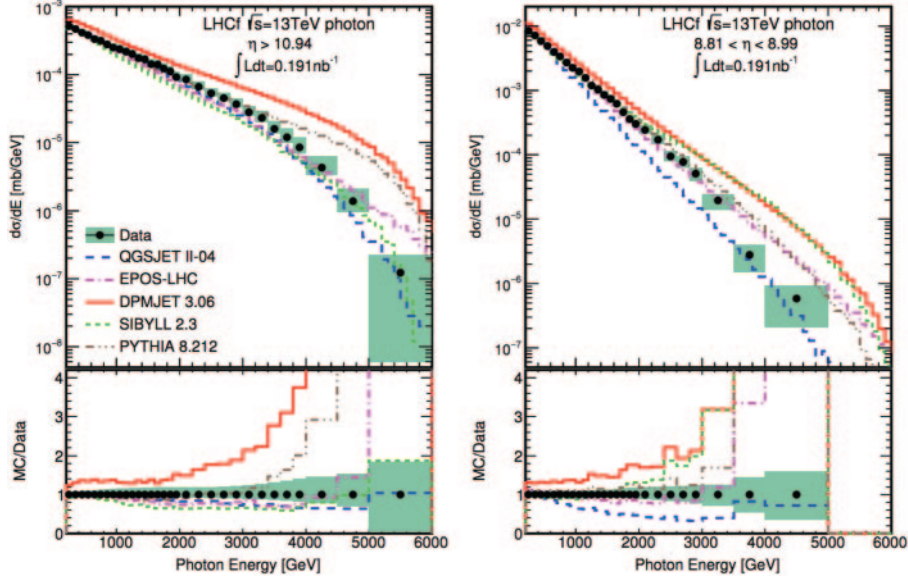


Fig. 3. – LHCf  $\gamma$  spectra in  $pp$  collisions at  $\sqrt{s} = 13$  TeV in two  $\eta$  ranges [32].

and  $n$ . In fig. 3 the energy distributions of  $\gamma$ 's in  $pp$  collisions at  $\sqrt{s} = 13$  TeV are compared with different simulations [32]. A similar behavior is observed at 7 TeV published in [33]. The behavior can be also compared with the  $\pi^0$  momentum distributions at 7 TeV [34]. None of the models are able to reproduce data in the whole  $\eta$  and energy, momentum ranges. The QGSJETII-04 reproduces relatively well the shapes for  $\gamma$  and  $\pi^0$ , but underestimates production at smaller  $\eta$ , while EPOS-LHC reproduces well the soft region, but overestimates data at higher energies. Similar to the  $\bar{p}$  the high energy tail of  $\gamma$  distribution measured in LHC  $pp$  collisions is more important due to falling CR spectra. The large part of this high energy  $\gamma$  is produced in diffraction. The diffraction contribution is apparently responsible for the  $\sim 15\%$  discrepancies in the diffusive  $\gamma$ -rays calculations with the QGSJET and parameterizations [35]. On the other hand the diffractive events can be measured at the LHCf by applying a veto on charged tracks from ATLAS at  $|\eta| < 2.5$ . In this measurement [36] the EPOS-LHC describes data relatively well, while QGSJETII-04 significantly underestimates the rate of such events at low energies. More discussion on the diffraction is given in the next sections.

The LHCf  $\pi^0$  measurements also allow to check different scaling hypothesis in the forward region, which is important for CR interactions [34]. The Feynman scaling states that the inelastic cross-section integrated in  $p_T$  is independent of the energy for the  $x_F$  parameter. The limiting fragmentation means that the rapidity distribution of produced particles is also independent on the energy in the forward region at  $y \sim y_{beam}$ . Then the  $p_T$  distribution of secondary particles in the fragmentation region should be independent of the energy. In the pQCD the scalings are violated due to gluon self-interactions, but this violation is related to soft-QCD effects, which are difficult to estimate. It is expected that smaller violations occur in the forward region [8]. The LHCf check of the scaling hypothesis is in reasonable agreement with RFT models, confirming that the scalings hold within 20% in the forward region up to  $\sqrt{s} = 7$  TeV.

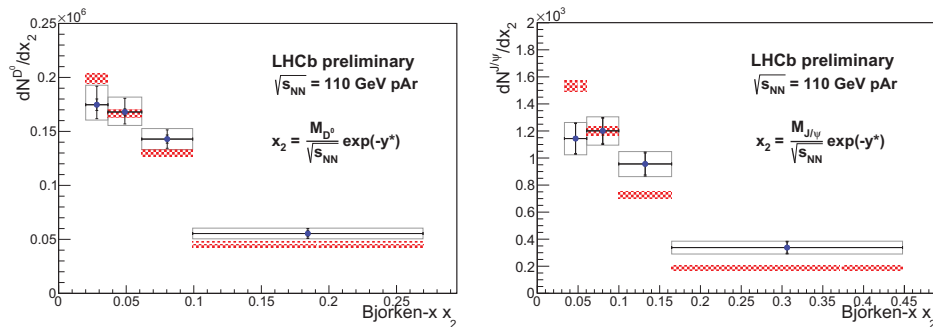


Fig. 4. – LHCb measurements of  $D_o$  (left) and  $J/\Psi$  (right) Bjorken- $x$  distributions in  $p\text{Ar}$  fixed target interactions at  $\sqrt{s} = 110.4$  GeV [42].

#### 4. – Neutrino

The production of  $\nu$  from the DM annihilation and from CR interactions is rather similar to  $\gamma$ -rays [37]. The main difference is an additional background for neutrino telescopes coming from the EAS neutrinos created by CR + air interactions. The hardest contribution is coming from decays of open charm mesons and baryons [38]. The LHCb charm measurements in  $pp$  collisions [39] significantly improve predictions for the charm production cross-sections [40]. In addition to the standard pQCD mechanism of charm production, the nonperturbative QCD contribution to the charm parton distribution function (PDF) at large  $x > 0.1$ , the so-called intrinsic charm, is favored by several experiments and theories [41]. This can significantly increase the neutrino flux from EAS and reduce the significance of the astrophysical  $\nu$  observations.

The LHCb measured the  $D_o$  and  $J/\Psi$  productions at large  $x$  in fixed target  $p\text{Ar}$  interactions at  $\sqrt{s} = 110.4$  GeV [42]. The simultaneous observation of the open charm and charmonium helps to disentangle the cold nuclear effects, such as antishadowing, which has similar signature to the intrinsic charm and will manifest in both cases at  $x_2 = 0.1\text{--}0.8$ . Figure 4 shows the Bjorken- $x_2$  distributions for  $D_o$  and  $J/\Psi$  in comparison with the standard PDF without intrinsic charm and cold nuclear effects. There is no evidence for the large intrinsic charm contribution.

Since the  $\gamma$ -rays above 10 TeV are absorbed in the galaxy via  $\gamma$ +ISRF  $e^\pm$  pair production, only  $\nu$  can trace CR sources at higher energies. Then the interactions of high energy astrophysical  $\nu$  with the ISG become very important. These interactions are sensitive to the PDF at low  $x \sim M_c^2/s < 10^{-5}$  accessible at LHCb via charm [39], low-mass Drell-Yan or central exclusive productions [43]. The LHCb measurements significantly improve the PDF fit at  $x < 10^{-5}$ , reducing uncertainties from more than 80% to about 20% [44].

#### 5. – Cross-section and diffraction

The RFT approach makes the calculation of the total cross-section possible. Various parameterizations based on the Donnachie-Landshoff model predict the power  $s^\epsilon$  ( $\epsilon = 0.08\text{--}0.12$ ) rise of the total cross-section driven by the pomeron exchange [45]. Most precise data are produced by the TOTEM Collaboration, which measured the total, inelastic and elastic cross-sections by different methods at different energies from

$\sqrt{s} = 1.8$  to 13 TeV [30]. These measurements impact all models used in CR physics, resulting in post-LHC tune [8]. Still there are large deviations between models in the  $\eta$  distribution of the produced particles even in the central region [46], and to a greater extent in the forward one [47], where the diffraction can contribute up to 50% at large  $x_F > 0.1$ . Since the simulation of soft diffraction processes is rather different from the hard central production, the diffraction has to be separated in inclusive production. The separation using the rapidity gap  $\Delta\eta = -\ln M_x^2/s$  can be nontrivial at LHC energies due to large fluctuations of nondiffractive inelastic interactions [48]. There is about 30% difference between the CMS and TOTEM measurements on the single diffraction (SD) in the  $M_x = 8\text{--}350$  GeV mass range [48, 49]. The QGSJET overestimates the low-mass SD measured at TOTEM, but underestimates the diffraction measured at CMS. The LHCf+ATLAS measurements of the enhanced diffractive  $\gamma$  production [36] and the LHCf measurements of neutrons [50] also favor a larger contribution from low-mass SD, similar to the CMS results. The EPOS-LHC reproduces the diffraction enhanced  $\gamma$  production, but fails to explain the LHCf neutron measurements. Both models fail to explain the SD  $\eta$  distribution measured by the TOTEM+ATLAS [47]. The measurements of diffractive contributions in different components will be an important test of RFT models and would reduce nuclear uncertainties in the CR forward productions.

## 6. – Summary

The LHC forward detectors provide valuable measurements at very low and very large Bjorken  $x$  at high energies, inaccessible in other experiments. These measurements are intensively used to validate the simulation models, which has to be used not only in the accelerator and EAS physics, but also in the simulation of CR interactions in space. At the same time, the parameterizations are needed to evaluate the uncertainties in predictions.

Recent improvements in modeling of CR interactions and reduction of nuclear uncertainties almost excluded the DM contribution to the measured  $\bar{p}$  flux in the 1–400 GeV range. The updated simulations of atmospheric  $\nu$  from EAS confirm the astrophysical origin of the observed high-energy neutrino  $E_\nu > 10^5$  eV. The nuclear uncertainties in the diffusive  $\gamma$ -rays production are not enough to explain the observed excess in the 1–100 GeV above galactic plane. Similarly, the CR positron excess cannot be explained by the secondary CR interactions. These  $\gamma$  and positron excesses with respect to the predictions, they both remain a puzzle still to be solved.

\* \* \*

The author thanks S. Ostapchenko, G. Graziani, L. Bonechi, T. Pierog, M. Winkler and M. Albrow for clarifying discussions.

## REFERENCES

- [1] KLASSEN M., POHL M. and SIGL G., *Prog. Part. Nucl. Phys.*, **85** (2015) 1.
- [2] AMS02 COLLABORATION, *Phys. Rev. Lett.*, **113** (2014) 121101.
- [3] AMS02 COLLABORATION, *Phys. Rev. Lett.*, **117** (2016) 091103.
- [4] FERMI-LAT COLLABORATION, *Astrophys. J.*, **793** (2014) 64.
- [5] STRONG A. W., MOSKALENKO I. V. and REIMER O., *Astrophys. J.*, **537** (2000) 763.
- [6] JOHANNESSON G. *et al.*, *Astrophys. J.*, **824** (2016) 16.
- [7] ALOISIO R., BLASI P., DE MITRI I. and PETRERA S., arXiv:1707.06147 (2017).

- [8] PIEROG T., *EPJ Web of Conferences*, **145** (2017) 18002.
- [9] PIEROG T., KARPENKO I., KATZY J. M. *et al.*, *Phys. Rev. C*, **92** (2015) 034906.
- [10] OSTAPCHENKO S., *Phys. Rev. D*, **83** (2011) 014018.
- [11] TOTEM COLLABORATION, CERN-LHCC-2014-021 (2014).
- [12] LHCf COLLABORATION, CERN-LHCC-2006-004 (2006).
- [13] LHCb COLLABORATION, *JINST*, **9** (2014) P12005.
- [14] ENTERRIA D. *et al.*, *Astropart. Phys.*, **35** (2011) 98.
- [15] KACHELRIESS M., MOSKALENKO I. and OSTAPCHENKO S., *Astrophys. J*, **803** (2015) 54.
- [16] REINERT A. and WINKLER M., *JCAP*, **01** (2018) 055.
- [17] TAN L. C. and NG L. K., *J. Phys. G: Nucl. Phys.*, **9** (1983) 1289.
- [18] DI MAURO M. *et al.*, *Phys. Rev. D*, **90** (2014) 085017.
- [19] WINKLER M., *JCAP*, **02** (2017) 048.
- [20] LHCb COLLABORATION, LHCb-CONF-2017-002 (2017).
- [21] FENG J. and ZHANG H., arXiv:1701.02263 (2017).
- [22] FISHER H. G. for NA49 COLLABORATION, *Acta Phys. Hung. A*, **17** (2003) 369.
- [23] KORSMEIER M., DONATO F. and di MAURO M., arXiv:1802.03030 (2018).
- [24] NERONOV A., SEMIKOZ D. V. and TAYLOR A. M., *Phys. Rev. Lett.*, **108** (2012) 051105.
- [25] STIPHENS S. A. and BADHWAR G. D., *Astrophys. Space Sci.*, **76** (1981) 213.
- [26] DERMER C. D., *Astron. Astrophys.*, **157** (1986) 223.
- [27] KAMAE T. *et al.*, *Astrophys. J*, **647** (2006) 692.
- [28] DERMER C. D., *EPJ Web of Conferences*, **105** (2015) 03001.
- [29] DELAHAYE T. *et al.*, *Astron. Astrophys.*, **531** (2011) A37.
- [30] TOTEM COLLABORATION, CERN-EP-2017-321 (2017).
- [31] SATO H., SHIBATA T. and YAMAZAKI R., *Astropart. Phys.*, **36** (2012) 83.
- [32] LHCf COLLABORATION, *Phys. Lett. B*, **780** (2018) 233.
- [33] LHCf COLLABORATION, *Phys. Lett. B*, **715** (2012) 298.
- [34] LHCf COLLABORATION, *Phys. Rev. D*, **94** (2016) 032007.
- [35] KACHELRIESS M. and OSTAPCHENKO S., *Phys. Rev. D*, **86** (2012) 043004.
- [36] LHCf and ATLAS COLLABORATIONS, ATLAS-CONF-2017-075 (2017).
- [37] KACHELRIESS M. and OSTAPCHENKO S., *Phys. Rev. D*, **90** (2014) 083002.
- [38] ICECUBE COLLABORATION, *Eur. Phys. J. C*, **77** (2017) 692.
- [39] LHCb COLLABORATION, *JHEP*, **03** (2016) 159.
- [40] BHATTACHARYA A. *et al.*, *JHEP*, **11** (2016) 167.
- [41] LAHA R. and BRODSKY S., *Phys. Rev. D*, **96** (2017) 123002.
- [42] LHCb COLLABORATION, LHCb-CONF-2017-001 (2017).
- [43] LHCb COLLABORATION, *Acta Phys. Pol. Suppl.*, **8** (2015) 861.
- [44] PROSA COLLABORATION, *Eur. Phys. J. C*, **75** (2015) 396.
- [45] COMPETE COLLABORATION, *Phys. Rev. Lett.*, **89** (2002) 201801.
- [46] CMS and TOTEM COLLABORATIONS, *Eur. Phys. J. C*, **74** (2014) 3053.
- [47] TOTEM COLLABORATION, *Eur. Phys. J. C*, **75** (2015) 126.
- [48] KHOZE V. A., MARTIN A. D. and RYSKIN M. G., *Int. J. Mod. Phys. A*, **30** (2015) 1542004.
- [49] OSTAPCHENKO S., *Phys. Rev. D*, **89** (2014) 074009.
- [50] LHCf COLLABORATION, *Phys. Lett. B*, **750** (2015) 360.